1.84 μm emission of Tm^{3+} sensitized by Yb^{3+} ions in monoclinic $KGd(WO_4)_2$ single crystals

F. Güell,[a] J. Massons, Jna. Gavaldà, M. C. Pujol, M. Aguiló, and F. Díaz
Física i Cristallografia de Materials (FiCMA), Universitat Rovira i Virgili, Campus Sescelades, C/Marcellí Domingo, s/n, E-43007 Tarragona, Catalunya, Spain

(Received 4 October 2006; accepted 22 November 2006; published online 6 February 2007)

By exciting at 940 nm, we have characterized the 1.84 μm near infrared emission of trivalent thulium ions in Yb^{3+}, Tm^{3+}:$KGd(WO_4)_2$ single crystals as a function of the dopant concentration and temperature, from 10 K to room temperature. An overall $^3H_6$ Stark splitting of ~470 cm^{-1} for the Tm^{3+} ions in the Yb^{3+}, Tm^{3+}:$KGd(WO_4)_2$ was obtained. We also studied the blue emission at 476 nm (Tm^{3+}) and the near infrared emissions at 1.48 μm (Tm^{3+}) and 1 μm (Yb^{3+}) as a function of the dopant concentration. Experimental decay times of the $^1G_4$, $^3H_4$, and $^3F_4$ (Tm^{3+}) and $^2F_{5/2}$ (Yb^{3+}) excited states have been measured as a function of Yb^{3+} and Tm^{3+} ion concentrations. For the $^3F_4 \rightarrow {}^3H_6$ transition of Tm^{3+} ions, we used the reciprocity method to calculate the maximum emission cross section of 3.07×10^{-20} cm^2 at 1.84 μm for the polarization parallel to the N_m principal optical direction. © *2007 American Institute of Physics*. [DOI: 10.1063/1.2433131]

I. INTRODUCTION

Diode-pumped solid-state lasers operating in the eye-safe 2 μm spectral region have applications in a number of important areas because water has a strong optical absorption band at this wavelength. Potential applications lie in the fields of medicine, laser radar [light detection and ranging (LIDAR)], and atmosphere monitoring. Tm^{3+}-doped laser materials are emerging as sources of light with a broad tunability around 2 μm on the $^3F_4 \rightarrow {}^3H_6$ transition. Yb^{3+} ions have an extremely simple energy level scheme with only one excited state, $^2F_{5/2}$, above the ground state, $^2F_{7/2}$. An advantage of Yb^{3+}-codoped materials is the intense absorption band around 1 μm, which allows them to be pumped with an efficient high-power InGaAs laser diode. $KGd(WO_4)_2$ (KGW) single crystals are very attractive materials as laser hosts.[1] Their monoclinic structure provides an appreciable optical anisotropy suitable for obtaining polarized laser radiation.[2] They are easily grown and Gd^{3+} can be efficiently substituted by Yb^{3+} and Tm^{3+} ions.[3]

An early demonstration of Tm^{3+} lasing on the $^3F_4 \rightarrow {}^3H_6$ transition in monoclinic double tungstates was realized in 1997 with Xe-flash lamp pumping in which 0.5 at. % Tm^{3+}:$KY(WO_4)_2$ and 0.5 at. % Tm^{3+}:KGW rods sensitized with 5 at. % Er^{3+} and 5 at. % Yb^{3+} operated at cryogenic temperatures and laser output wavelengths of 1.92 and 1.93 μm, respectively.[4] Soon afterwards, cw room temperature operation of highly doped 15 at. % Tm^{3+}:$KY(WO_4)_2$ was demonstrated with longitudinal Ti:sapphire laser pumping near 800 nm.[5] They found that the thulium concentration must be high enough to ensure efficient pumping, but low enough to minimize concentration quenching effects due to cross-relaxation-type ($^3H_4 + {}^3H_6 \rightarrow {}^3F_4 + {}^3F_4$) and nonradiative energy transfer between active ions. In 2002, Yb^{3+}, Tm^{3+}:$KY(WO_4)_2$ was studied for InGaAs diode pumping at 980 nm with subsequent excitation transfer from Yb^{3+} to Tm^{3+} ions at several dopant concentrations.[6,7] Recently, we demonstrated the successful crystal growth of Tm^{3+}:KGW and studied its spectroscopic properties.[8] We obtained highly efficient tunable laser operation in the cw regime at room temperature on the $^3F_4 \rightarrow {}^3H_6$ transition.[9]

In this paper, we have characterized the near infrared emission at 1.84 μm of thulium ions in KGW single crystals codoped with Yb^{3+} and Tm^{3+} ions by pumping at 940 nm. We analyzed luminescence as a function of Yb^{3+} and Tm^{3+} ion concentrations and temperature. The reciprocity method has been used to calculate the 1.84 μm emission cross section from the absorption cross section and to compare it with the experimental results. The decay times corresponding to the emitting levels $^1G_4$, $^3H_4$, and $^3F_4$ (Tm^{3+}) and $^2F_{5/2}$ (Yb^{3+}) were measured at several Yb^{3+} and Tm^{3+} ion concentrations.

II. EXPERIMENT

We grew good-optical-quality and inclusion-free single crystals of KGW codoped with Yb^{3+} and Tm^{3+} ions at several dopant concentrations by the top-seeded-solution-growth slow-cooling method (TSSG-SC) using $K_2W_2O_7$ as solvent according to the method described elsewhere.[10] Powdered precursors of Yb^{3+}, Tm^{3+}:KGW single crystals were K_2CO_3, Gd_2O_3, Tm_2O_3, Yb_2O_3, and WO_3 (Fluka, 99.9% pure). These were used to synthesize these types of single crystals at several Yb^{3+} and Tm^{3+} ion concentrations, $KGd_{1-x-y}Yb_xTm_y(WO_4)_2$, with a binary solution composition of 11.5 mol % solute/88.5 mol % solvent. Table I summarizes the dopant concentrations of Yb^{3+} and Tm^{3+} ions in the crystals measured by electron probe microanalysis (EPMA). The dopant concentrations in the solution are related to the total rare earth content. The substitution of the

[a]Electronic mail: frank.guell@urv.cat

TABLE I. Composition of the KGW single crystals.

$[Yb^{3+}]$	$[Tm^{3+}]$	$[Yb^{3+}]$	$[Tm^{3+}]$	Stoichiometric formula
(at. % in the solution)		($\times 10^{20}$ at./cm^3 in the crystal)		
0.5	0.5	0.57	0.44	$KGd_{0.984}Yb_{0.009}Tm_{0.007}(WO_4)_2$
1.5	0.5	0.82	0.38	$KGd_{0.982}Yb_{0.012}Tm_{0.006}(WO_4)_2$
2.5	0.5	1.39	0.38	$KGd_{0.972}Yb_{0.022}Tm_{0.006}(WO_4)_2$
5.0	0.5	2.33	0.38	$KGd_{0.957}Yb_{0.037}Tm_{0.006}(WO_4)_2$
2.5	1.5	1.32	0.88	$KGd_{0.965}Yb_{0.021}Tm_{0.014}(WO_4)_2$
5.0	1.5	2.21	0.88	$KGd_{0.951}Yb_{0.035}Tm_{0.014}(WO_4)_2$
5.0	2.5	2.33	1.26	$KGd_{0.943}Yb_{0.037}Tm_{0.020}(WO_4)_2$
7.5	2.5	3.41	1.32	$KGd_{0.925}Yb_{0.054}Tm_{0.021}(WO_4)_2$
10	2.5	5.55	1.58	$KGd_{0.887}Yb_{0.088}Tm_{0.025}(WO_4)_2$

rare earth in KGW for lanthanide ions was limited in the case of KGW by Yb^{3+} ions at 10 at. %, when cracks began to appear.

For the absorption measurements, we used the sample of $KGd_{0.957}Yb_{0.037}Tm_{0.006}(WO_4)_2$ with ytterbium and thulium concentrations of 5.0 and 0.5 at. % in the solution, respectively. We cut and polished the sample with the faces perpendicular to the principal optical directions, with a thickness of 4.73 mm for the N_m and 5.35 mm for the N_p. Optical absorption spectra were measured with a Varian CARY 500 scan spectrophotometer.

Emission spectra were obtained with an optical parametrical oscillator, VEGA 100, pumped by the third harmonic of a Q-switched Nd^{3+}:YAG (yttrium aluminum garnet) laser (pulse duration, 7 ns; repetition rate, 10 Hz), SAGA 120, from B.M. Industries. In order to compare the emission intensities of Yb^{3+} and Tm^{3+} ions in different samples, the measurements were performed under the same experimental conditions. Fluorescence was dispersed through a HR460 Jobin Yvon-Spex monochromator (focal length, 460 mm; $f/5.3$; spectral resolution, 0.05 nm). The gratings used were a 1800 groove/mm grating blazed at 1 μm and a 600 groove/mm grating blazed at 2 μm. The detectors applied were Hamamatsu R928 and R5509-72 photomultipliers and a P7163 InAs photovoltaic. These were connected to a Perkin Elmer 7265DSP lock-in amplifier. Lifetime measurements were taken at various Yb^{3+} and Tm^{3+} ion concentrations. Time decay curves were recorded using a Tektronix TDS-714 digital oscilloscope. For low temperature ($T \geqslant 10$ K) emission measurements, the samples were mounted into a closed cycle helium cryostat Oxford CCC1104.

III. RESULTS AND DISCUSSION

A. Spectra and luminescence intensities

By pumping at 940 nm, Yb^{3+} ions generated an emission observed around 1 μm, corresponding to the $^2F_{5/2} \rightarrow {}^2F_{7/2}$ transition. At this pump wavelength, Tm^{3+} ions generated emissions observed around 476 nm, 1.48 μm, and 1.84 μm, corresponding to the $^1G_4 \rightarrow {}^3H_6$, $^3H_4 \rightarrow {}^3F_4$, and $^3F_4 \rightarrow {}^3H_6$ transitions, respectively. We found that the intensities of these emissions were strongly affected by the concentrations of Yb^{3+} and Tm^{3+} ions. At a fixed Yb^{3+} concentration, the intensity of the Yb^{3+} ion emission decreased as the Tm^{3+} concentration increased. Figure 1 shows the RT emission spectra for the 1 μm emission, for samples with fixed 5.0 at. % Yb^{3+} and 0.5, 1.5, and 2.5 at. % Tm^{3+} ion concentrations. Since the emission intensity around 1 μm decreases with increasing Tm^{3+} ion concentration, the probability of energy transfer from Yb^{3+} to Tm^{3+} ions is demonstrated to be very high, as observed in other works.[11]

At a fixed Tm^{3+} concentration, the intensity of Tm^{3+} ion emissions increased as Yb^{3+} concentration increased. Also, at a fixed Yb^{3+} concentration, the intensity of Tm^{3+} ion emissions increased as Tm^{3+} concentration increased. Therefore, the intensity of Tm^{3+} ion emissions increased as Yb^{3+} and Tm^{3+} ion concentrations increased. Quenching phenomena of thulium luminescence due to higher Yb^{3+} and Tm^{3+} ion concentrations were not observed in the samples we studied. Figure 2 shows the RT emission spectra for the 476 nm, 1.48 μm, and 1.84 μm emissions, for samples with 5, 7.5, and 10 at. % Yb^{3+} and fixed 2.5 at. % Tm^{3+} ion concentrations. Maximum emission intensity was found in samples containing 10 at. % Yb^{3+} and 2.5 at. % Tm^{3+} ion concentrations.

We also analyzed the evolution with temperature of the 1.84 μm emission channel corresponding to the $^3F_4 \rightarrow {}^3H_6$ transition for a 10 at. % Yb^{3+} and 2.5 at. % Tm^{3+} sample. Figure 3 shows the temperature dependence of the 1.84 μm emission spectrum from 10 K to RT. We labeled the n Stark levels, increasing from 0 to n in energy, n' for the upper level

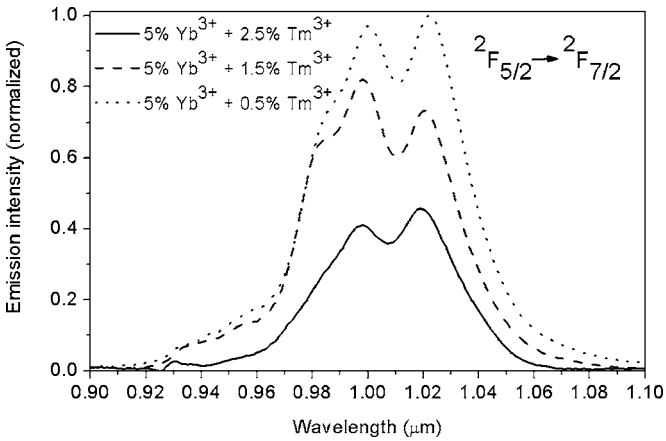

FIG. 1. Room temperature spectra of the emission of Yb^{3+} ions as a function of the combined Yb^{3+} and Tm^{3+} dopant concentration in KGW single crystals by exciting at 940 nm.

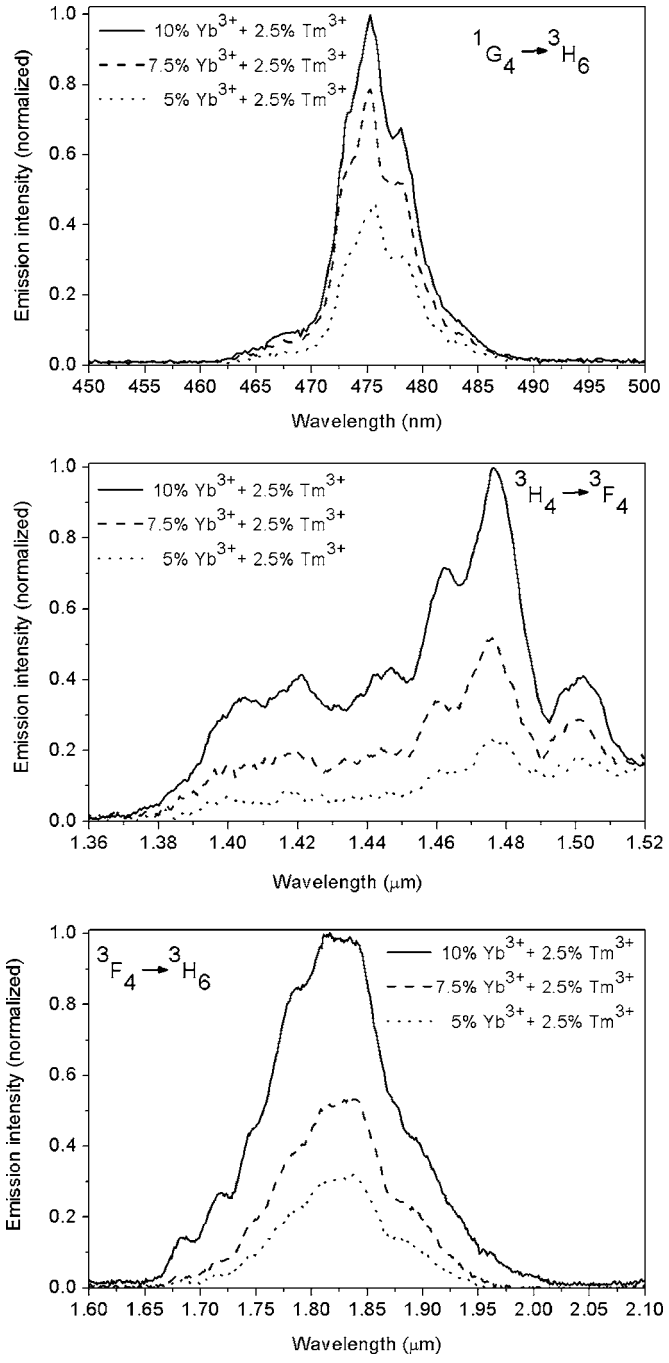

FIG. 2. Room temperature spectra of the 476 nm (a), 1.48 μm (b), and 1.84 μm (c) emissions of Tm^{3+} ions as a function of the combined Yb^{3+} and Tm^{3+} dopant concentration in KGW single crystals by exciting at 940 nm.

and n for the lower level. We observed seven peaks: at 1.770, 1.790, 1.808, 1.845, 1875, 1913, and 1.931 μm at 10 K, which correspond to the electronic transitions $^3F_4(0') \rightarrow {}^3H_6(0)$, $^3F_4(0') \rightarrow {}^3H_6(1)$, $^3F_4(0') \rightarrow {}^3H_6(3)$, $^3F_4(0') \rightarrow {}^3H_6(7)$, $^3F_4(0') \rightarrow {}^3H_6(10)$, $^3F_4(0') \rightarrow {}^3H_6(11)$, and $^3F_4(0') \rightarrow {}^3H_6(12)$, respectively. These Stark sublevels of the ground state $^3H_6$ are located at 0, 69, 119, 227, 315, 427, and 470 cm^{-1}, respectively. At 50 K we identified new peaks at 1.745, 1.755, 1.782, and 1.901 μm that appeared due to the thermal population of the upper Stark levels of the $^3F_4$ excited state. From the $^3F_4$ Stark splitting obtained in our previous work,[12] these peaks correspond to the $^3F_4(3') \rightarrow {}^3H_6(0)$, $^3F_4(2') \rightarrow {}^3H_6(0)$, and $^3F_4(5') \rightarrow {}^3H_6(10)$, transitions, respectively. All these results show a small shift from the corresponding energies of the Stark sublevels of the $^3H_6$ ground state in Tm^{3+}-doped KGW single crystals[13] due to the incorporation of Yb^{3+} ions in the lattice.

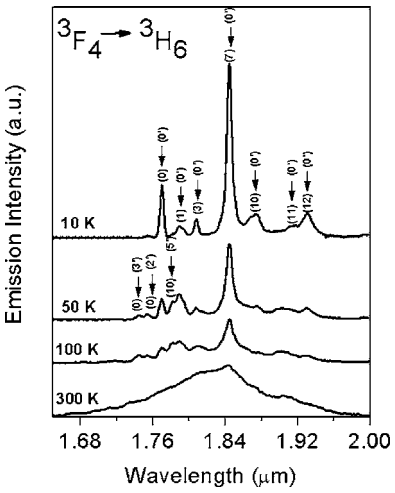

FIG. 3. Temperature evolution of the 1.84 μm emission of Tm^{3+} ions in 10 at. %, Yb^{3+}, 2.5 at. % Tm^{3+}:KGW single crystals.

Figure 4 shows a partial energy level diagram of Yb^{3+} and Tm^{3+} ions in KGW single crystals,[13,14] the possible energy transfer processes and the luminescence channels investigated. The ytterbium pump process and the luminescence channels are marked by solid arrows. The energy transfer processes from Yb^{3+} to Tm^{3+} ions and the cross-relaxation mechanisms within the Tm^{3+} energy levels are marked by dash and dot arrows. The pumping at 940 nm excited only the Yb^{3+} ions; the electronic population was excited from the ground state $^2F_{7/2}$ to the $^2F_{5/2}$ energy level. The decay from the $^2F_{5/2}$ to the $^2F_{7/2}$ energy levels of Yb^{3+} ions generated an emission around 1 μm. Two Yb^{3+} ions in its excited state $^2F_{5/2}$ transferred their energy to the $^1G_4$ energy level of Tm^{3+} ions ($^2F_{5/2} + {}^2F_{5/2} + {}^3H_6 \rightarrow {}^2F_{7/2} + {}^2F_{7/2} + {}^1G_4$) (see Fig. 4).[11,15] The decay from the $^1G_4$ to the $^3H_6$ energy levels of Tm^{3+} ions generated the emission around 476 nm. Emissions around 1.48 and 1.84 μm were generated due to the decay from the $^3H_4$ to the $^3F_4$ and the $^3F_4$ to the $^3H_6$ energy levels of Tm^{3+} ions, respectively. The $^3F_4$ energy level of Tm^{3+} ions is also populated via two cross-relaxation mechanisms through the phonon-assisted self-quenching process ($^1G_4 + {}^3H_6 \rightarrow {}^3F_2 + {}^3F_3 + {}^3F_4$ and $^3H_4 + {}^3H_6 \rightarrow {}^3F_4 + {}^3F_4$) (see Fig. 4).[16] The effectiveness of this quenching process increases with higher thulium concentrations. Note that we have two steady-state population inversions on the $^3H_4 \rightarrow {}^3F_4$ and $^3F_4 \rightarrow {}^3H_6$ transitions.

B. Dynamics of the Yb^{3+}–Tm^{3+} energy transfer

We investigated the lifetime of the $^1G_4$, $^3H_4$, and $^3F_4$ (Tm^{3+}) and $^2F_{5/2}$ (Yb^{3+}) emitting levels as a function of Yb^{3+} and Tm^{3+} ion concentrations. Table II summarizes the results obtained. The experimental lifetimes of the $^1G_4$ and $^3H_4$ states decreased strongly as thulium concentration increased (see Table II). This is explained by the very efficient energy transfer mechanisms between thulium ions. The lifetimes of

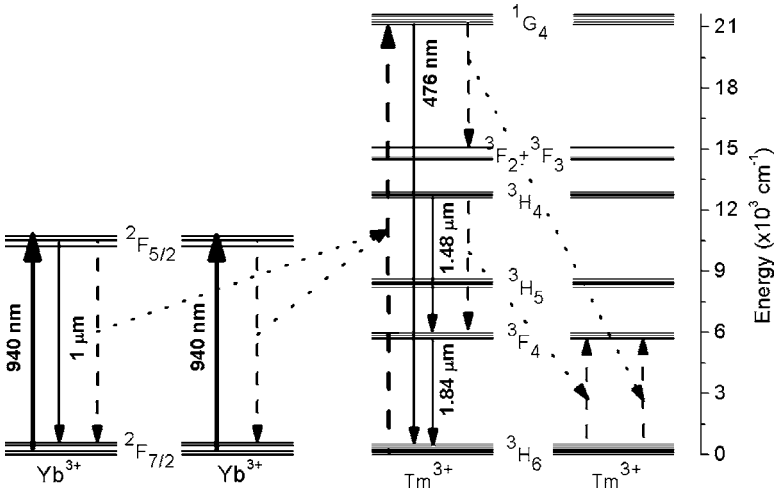

FIG. 4. Partial energy level scheme, energy transfer processes, and luminescence channels studied in Yb^{3+}, Tm^{3+}:KGW single crystals.

the $^1G_4$ and $^3H_4$ (Tm^{3+}) and $^2F_{5/2}$ (Yb^{3+}) energy levels for samples with fixed 5 at. % Yb^{3+} and 0.5, 1.5, and 2.5 at. % Tm^{3+} ion concentrations are shown in Fig. 5. It can be seen that the lifetime decreases with increasing Tm^{3+} ion concentration, which shows that the cross relaxation has a considerable effect on the lifetime of $^1G_4$ and $^3H_4$ energy levels and demonstrates the energy transfer from Yb^{3+} to Tm^{3+} ions due to the decrease in the lifetime of $^2F_{5/2}$ energy level. This transfer becomes more efficient with higher concentrations of acceptor ions and hence by a large thulium concentration.

The lifetimes of the $^1G_4$ and $^3H_4$ (Tm^{3+}) and $^2F_{5/2}$ (Yb^{3+}) energy levels for samples with 5, 7.5, and 10 at. % Yb^{3+} and fixed 2.5 at. % Tm^{3+} ion concentrations are shown in Fig. 6. The figure illustrates that the lifetime is almost independent of the Yb^{3+} ion concentration for the $^1G_4$ and $^3H_4$ energy levels. Accordingly, it is considered that no energy back transfer from Tm^{3+} to Yb^{3+} ions occurs involving the $^1G_4$ and $^3H_4$ energy levels. For the $^2F_{5/2}$ energy level, the lifetime decreases with increasing Yb^{3+} ion concentration, so the energy transfer from Yb^{3+} to Tm^{3+} ions could also be enhanced by a large ytterbium concentration. The reported value of luminescence lifetime of 2 at. % Yb^{3+} in KGW single crystals is 304 μs,[17] whereas we measured 246 μs with a sample containing 2.5 at. % of Yb^{3+} and 1.5 at. % of Tm^{3+}. The shortening of Yb^{3+} lifetime in the presence of thulium is evidence that the energy transfer process is nonradiative, as was also observed in YVO_4 single crystals codoped with Yb^{3+} and Tm^{3+} ions.[18]

The decay times of the $^3F_4$ energy level, which is the upper level for laser operation around 2 μm, for samples with fixed 5 at. % Yb^{3+} and 0.5, 1.5, and 2.5 at. % Tm^{3+} ion concentrations are 1730, 1690, and 1560 μs. The decrease of the measured lifetime with increasing thulium concentration is due to the energy migration within the thulium ions. The experimental lifetimes of the $^3F_4$ state are of the order of milliseconds because it is depopulated to the ground state $^3H_6$ by predominantly radiative decay. So the $^3F_4$ state is the storage reservoir and would be interesting for laser operation because of its long lifetime.

C. Calculated emission and gain cross sections for the 1.84 μm emission

One of the most important parameters influencing the laser performance of a material is the stimulated emission cross section (σ_e). We calculated the emission cross-section spectra of the $^3F_4 \rightarrow {}^3H_6$ transition using the so-called reciprocity method (RM).[19] The emission cross section (σ_e) is calculated from the absorption cross section (σ_a) and the splitting of the energy levels using the following equation:

$$\sigma_e(\nu) = \sigma_a(\nu)\frac{Z_l}{Z_u}\exp\left[\frac{(E_{\mathrm{ZL}} - h\nu)}{k_B T}\right], \tag{1}$$

where Z_l and Z_u are the partition functions and E_{ZL} is the zero line or energy separation between the lowest energy sublevels of the ground state (lower) and the first excited state (upper), respectively. The partition functions are calculated from

TABLE II. Experimental decay times of the $^2F_{5/2}$ (Yb^{3+}) and $^1G_4$, $^3H_4$, and $^3F_4$ (Tm^{3+}) energy levels in KGW single crystals as a function of Yb^{3+} and Tm^{3+} ion concentrations.

[Yb^{3+}] (at. % in the solution)	0.5	1.5	2.5	5.0	2.5	5.0	5.0	7.5	10.0
[Tm^{3+}] (at. % in the solution)	0.5	0.5	0.5	0.5	1.5	1.5	2.5	2.5	2.5
τ ($^2F_{5/2}$(μs))	292	275	311	288	246	218	166	141	117
τ ($^1G_4$(μs))	191	181	183	200	153	141	108	106	103
τ ($^3H_4$(μs))	314	283	269	274	254	252	185	178	176
τ ($^3F_4$(μs))	⋯	⋯	⋯	1730	1770	1690	1560	1580	1610

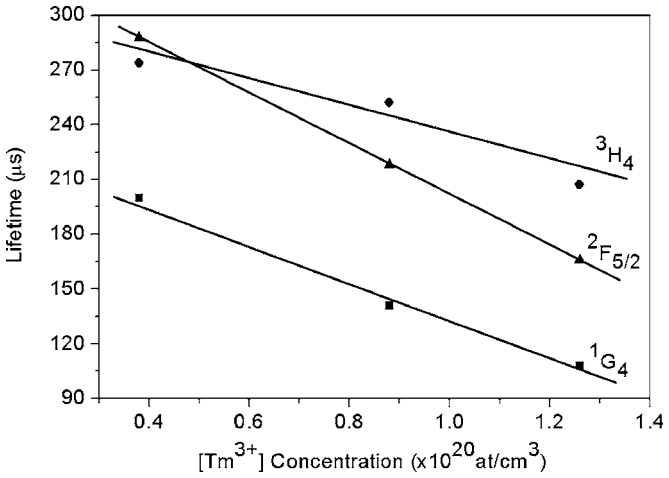

FIG. 5. Tm^{3+} ion concentration dependence of the lifetime of the $^2F_{5/2}$ (Yb^{3+}) and $^1G_4$ and $^3H_4$ (Tm^{3+}) energy levels at fixed 5.0 at. % Yb^{3+}.

$$Z = \sum_k d_k \exp\left[\frac{-E_k}{k_B T}\right], \tag{2}$$

where d_k and the E_k are the degeneracies and the energies, respectively, of each sublevel of the upper and lower energy levels involved. In our case, the ratio Z_l/Z_u was 1.21 and E_{ZL} was 5651 cm^{-1}. Figure 7 shows the calculated emission and experimental absorption cross sections for polarizations $E\|N_m$ and $E\|N_p$ of the $^3F_4 \rightarrow {}^3H_6$ transition at RT in the 1.5–2 μm range. The maximum absorption cross sections are 3.07×10^{-20} cm^2 for the polarization $E\|N_m$ at 1.840 μm and 1.73×10^{-20} cm^2 for the polarization $E\|N_p$ at 1.756 μm. The maximum emission cross sections are 3.07×10^{-20} cm^2 for the polarization $E\|N_m$ at 1.840 μm and 1.73×10^{-20} cm^2 for the polarization $E\|N_p$ at 1.756 μm. For polarization $E\|N_g$ the absorption and emission cross sections are much lower than for polarizations $E\|N_m$ and $E\|N_p$, and consequently such orientation is not attractive for laser operation. Figure 7 shows that these spectra exhibit the characteristic optical anisotropy of the host KGW, where the spectrum for the $E\|N_m$ polarization is the most intense, resulting in the highest possibility of obtaining polarized stimulated

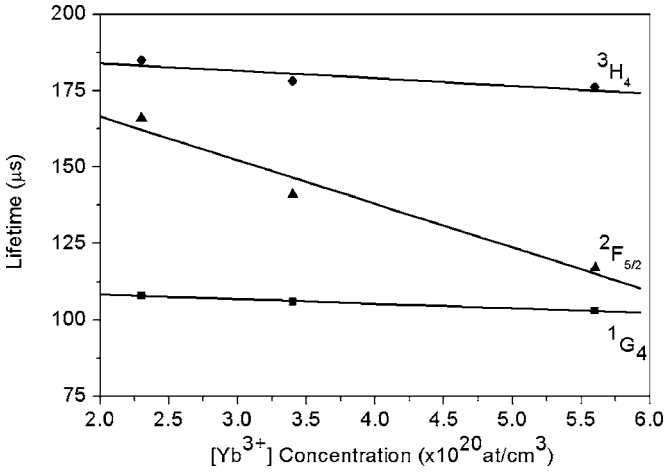

FIG. 6. Yb^{3+} ion concentration dependence of the lifetime of the $^2F_{5/2}$ (Yb^{3+}) and $^1G_4$ and $^3H_4$ (Tm^{3+}) energy levels at fixed 2.5 at. % Tm^{3+}.

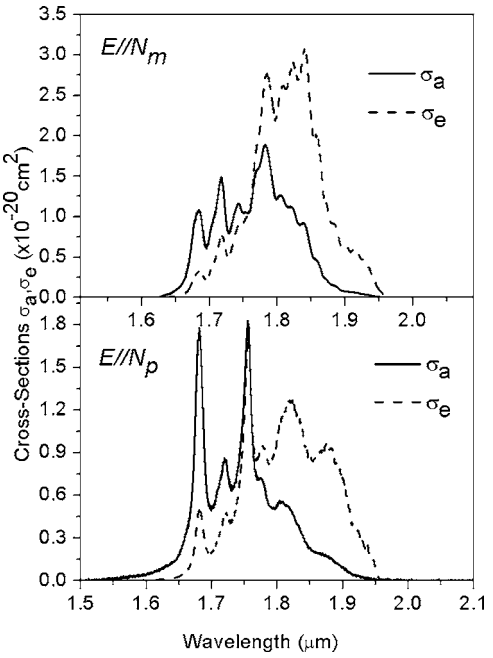

FIG. 7. Absorption cross sections at RT σ_a corresponding to the $^3H_6 \rightarrow {}^3F_4$ transition recorded for polarizations $E\|N_m$ and $E\|N_p$ (solid lines) and emission cross sections σ_a (dashed lines) calculated using the reciprocity method.

emission. These absorption and emission cross-section spectra will be useful for designing and modeling cw and pulsed lasers.

The $^3F_4 \rightarrow {}^3H_6$ transition corresponds to a quasi-three-level laser scheme in which the lower level is thermally populated at RT. This results in considerable reabsorption and an increased threshold for laser operation. Reducing reabsorption and maintaining efficient absorption of the pump light is one of the key issues in the design of thulium-doped laser systems at this transition. The reabsorption processes of the 1.84 μm emission by resonant transitions occur when absorption and emission overlapping is important. As a first approximation, the threshold for light amplification is achieved when the emitted light counterbalances the absorption losses. If β is the population inversion rate, the gain cross section can be calculated using $\sigma_{gain}=\beta\sigma_e-(1-\beta)\sigma_a$, where σ_e and σ_a are the emission and absorption cross sections derived from the RM, respectively, and σ_{gain} is the effective emission cross section. Figure 8 shows the gain cross sections calculated for several values of the parameter β for $E\|N_m$ and $E\|N_p$ polarizations in the 1.7–2 μm spectral region for the $^3F_4 \rightarrow {}^3H_6$ transition. The figure shows that, in general, the gain for $E\|N_m$ is higher. For a population inversion level of 0.2, the gain produced is in the 1.85–1.96 μm range. The higher energy limit of this interval increased when the population inversion level was increased, reaching up to 1.76 μm for a population inversion level of 0.5. For this level the maximum gain cross-section values were 1.09×10^{-20} cm^2 at 1.84 μm for $E\|N_m$ and 0.39×10^{-20} cm^2 at 1.88 μm for $E\|N_p$.

By averaging $\sigma_e(\nu)$ over the polarizations it is possible to obtain an estimation for the radiative lifetime (τ_{rad}) of the $^3F_4$ energy level using the Füchtbauer-Ladenburg equation.[20]

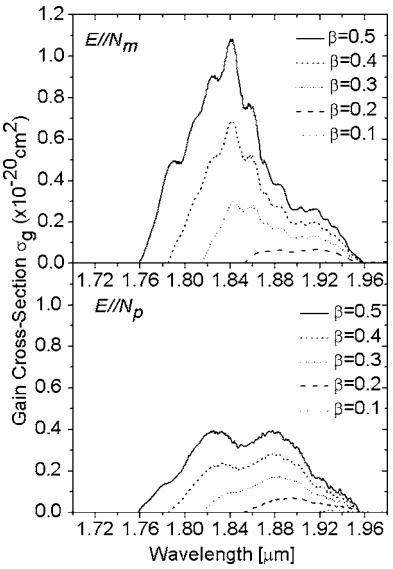

FIG. 8. Gain cross sections of the 1.84 μm emission at RT for polarizations $E\|N_m$ and $E\|N_p$ at several inversion population rates.

The error originating from the thermal distribution of the population in the ground state $^3H_6$ at room temperature when calculating $\sigma_a(\nu)$ can be suppressed by integrating the corresponding equation over the frequency[21]

$$\frac{1}{\tau_{\text{rad}}} = 8\pi n^2 \int \frac{\langle \sigma_e(\nu) \rangle}{\lambda^2} d\nu, \tag{3}$$

where $\langle\ \rangle$ denotes averaging over the polarizations. Using the $\sigma_e(\nu)$ dependence as calculated with the reciprocity method (Fig. 7) we thus arrive at $\tau_{\text{rad}}=1280$ μs at room temperature for 5.0 at. % Yb^{3+} and 0.5 at. % Tm^{3+} ion concentrations. The measured value is $\tau=1730$ μs (see Table II). To compare the potential laser capabilities of different media it is better to use the characteristic value $\sigma_e\tau$ [the laser threshold is proportional to $(\sigma_e\tau)^{-1}$]. This value is 5.31×10^{-20} cm^2 ms for polarization $E\|N_m$ and is therefore higher than the one for Tm^{3+}:YAG ($\sigma_e\tau=2.31\times10^{-20}$ cm^2 ms), which is one of the most efficient thulium laser systems.[22]

IV. CONCLUSIONS

In conclusion, we studied the 1.84 μm near infrared emission as a function of the dopant concentration and temperature pumping at 940 nm. Maximum emission intensity was found in samples containing 10 at. % Yb^{3+} and 2.5 at. % Tm^{3+} ion concentrations. From the polarized RT optical absorption measurements, we calculated the stimulated emission cross section using the reciprocity method. The maximum emission cross sections are 3.07×10^{-20} cm^2 at 1.840 μm and 1.9×10^{-20} cm^2 at 1.756 μm for the polarization parallel to the N_m and N_p principal optical directions, respectively. We were therefore able to calculate the optical gain for several population inversion rates and determine the spectral region in which light amplification is possible for future laser experiments using this material. From the gain versus wavelength characteristics, we found a tunability range of more than 300 nm for the $^3F_4 \rightarrow {}^3H_6$ transition. The lifetimes of the $^1G_4$, $^3H_4$, and $^3F_4$ (Tm^{3+}) and $^2F_{5/2}$ (Yb^{3+}) energy levels have been determined as a function of the dopant concentration. The results are discussed in detail. The lifetimes of the $^3G_4$ and $^3H_4$ energy levels were shortened with increasing thulium and ytterbium concentrations by cross-relaxation mechanisms between thulium ions. The very long lifetime of the $^3F_4$ energy level of thulium in KGW shows that easy population inversion is expected. This is needed for generating laser radiation. Our promising results encourage us to continue our research into the laser action of thulium in KGW single crystals codoped with Yb^{3+} and Tm^{3+} ions for the 1.84 μm emission.

ACKNOWLEDGMENTS

We gratefully acknowledge financial support from CICyT under Project Nos. JCI-2005-1924-13, MAT2005-06354-C05-03, MAT2004-20471-E, and FiT-020400-2005-14, from the EU-Commission Project DT-CRYS (STRP—NMP3-CT-2003-505580), and from CIRIT under Project No. 2005SGR658.

[1] A. A. Kaminskii, *Crystalline Lasers: Physical Processes and Operating Schemes* (CRC, Boca Raton, FL, 1996).
[2] M. C. Pujol, X. Mateos, R. Solé, J. Massons, J. Gavaldà, X. Solans, F. Díaz, and M. Aguiló, J. Appl. Crystallogr. **34**, 1 (2001).
[3] M. C. Pujol, R. Solé, J. Gavaldà, M. Aguiló, F. Díaz, V. Nikolov, and C. Zaldo, J. Mater. Res. **14**, 3739 (1999).
[4] A. A. Kaminskii, L. Li, A. V. Butashin, V. S. Mironov, A. A. Pavlyuk, S. N. Bagaev, and K. Ueda, Jpn. J. Appl. Phys., Part 2 **36**, L107 (1997).
[5] S. N. Bagaev, S. M. Vatnik, A. P. Maiorov, A. A. Pavlyuk, and D. V. Plakushchev, Quantum Electron. **30**, 310 (2000).
[6] A. A. Demidovich, A. N. Kuzmin, N. K. Nikeenko, A. N. Titov, M. Mond, and S. Kueck, J. Alloys Compd. **341**, 124 (2002).
[7] L. E. Batay, A. A. Demidovich, A. N. Kuzmin, A. N. Titov, M. Mond, and S. Kück, Appl. Phys. B: Lasers Opt. **75**, 457 (2002).
[8] F. Güell, Jna. Gavaldà, R. Solé, M. Aguiló, F. Díaz, M. Galán, and J. Massons, J. Appl. Phys. **95**, 919 (2004).
[9] V. Petrov, F. Güell, J. Massons, Jna. Gavaldà, R. Solé, M. Aguiló, F. Díaz, and U. Griebner, IEEE J. Quantum Electron. **40**, 1244 (2004).
[10] M. C. Pujol, M. Aguiló, F. Díaz, and C. Zaldo, Opt. Mater. (Amsterdam, Neth.) **13**, 33 (1999).
[11] J. Qiu and Y. Kawamoto, J. Appl. Phys. **91**, 954 (2002).
[12] F. Güell, R. Solé, Jna. Gavaldà, M. Aguiló, M. Galán, F. Díaz, and J. Massons, Opt. Mater. (Amsterdam, Neth.) (accepted).
[13] F. Güell, X. Mateos, R. Solé, Jna. Gavaldà, M. Aguiló, F. Díaz, and J. Massons, J. Lumin. **106**, 109 (2004).
[14] N. V. Kuleshov, A. A. Lagatsky, A. V. Podlipensky, V. P. Mikhailov, and G. Huber, Opt. Lett. **17**, 1317 (1997).
[15] X. Pei, Y. Hou, S. Zhao, Z. Xu, and F. Teng, Mater. Chem. Phys. **90**, 270 (2005).
[16] I. R. Martín, C. Goutaudier, S. Guy, Y. Guyot, G. Boulon, M. T. Cohen-Adad, and M. F. Joubert, Phys. Rev. B **60**, 7252 (1999).
[17] V. E. Kisel, A. E. Troshin, V. G. Shcherbitskz, and N. V. Kuleshov, ASSP 2004 (unpublished), Paper No. WB7.
[18] R. Lisiecki, G. Dominiak-Dzik, T. Lukasiewicz, and W. Ryba-Romanowski, J. Mol. Struct. **704**, 323 (2004).
[19] D. E. McCumber, Phys. Rev. **136**, A954 (1964).
[20] L. D. Deloach, S. A. Payne, L. L. Chase, L. K. Smith, W. L. Kway, and W. F. Krupke, IEEE J. Quantum Electron. **29**, 1179 (1993).
[21] F. D. Patel, E. C. Honea, J. Speth, S. A. Payne, R. Hutcheson, and R. Equal, IEEE J. Quantum Electron. **37**, 135 (2001).
[22] S. A. Payne, L. L. Chase, L. K. Smith, W. L. Kway, and W. F. Krupke, IEEE J. Quantum Electron. **28**, 2619 (1992).